4. Technological Applications - Nanotechnology

Nanotechnology is the meeting ground where today's industrial needs converge with fundamental sciences involving the nanoscale between atomistic and phenomenological theories. Technologies that could benefit from the nanoscale are manifold. They are situated in many areas, such as manufacturing, electronics, pharma and chemicals, biotechnology, and energy related disciplines.

A lot is expected from this new science and technology (c.f. Table 1). In manufacturing, for instance, one expects from the nanoscale to increase the performance of materials, and to discover and profit from unique material and transport properties. Nanostructured materials and processes are estimated to increase their market impact to about $ 340 billion per year in the next 10 years (Hitachi Reseach Institute, 2001). In the pharmaceutical industry one predicts that half of the production will dependent on nanotechnology in 10 to 15 years (Roco, Kluwer, 2001). Improved catalytic processes based on nanoscience will impact $ 100 billion per year in the next two decades (Roco, Kluwer, 2001). It is expected that lighter and more durable materials can be processed. Improvements in renewable energy sources such as solar cells, and water filtration and desalination systems are anticipated. The projection is that in 10 to 15 years nanoscience and nanotechnology will reduce the worldwide consumption of energy by more than 10 %, which corresponds to a reduction of 200 million tons of carbon emission ("NNI: The Initiative and Its Implementation Plan," p. 93).

Table 4-1: Expectations from Nanotechnology
(Source: Roco and W. S. Bainbridge, Societal Implications of Nanoscience and Nanotechnology, Kluwer)

Affected Areas	**Impact**	**Economical impact per year** (in 10 to 15 years)
Manufacturing	- Nanostructuring - Materials properties	$ 340 billion per year
Electronics	- Materials - Structure	$ 300 billion per year
Pharma		$ 180 billion per year
Chemicals	- Nanostructured catalyst	$ 100 billion per year
Transportation	- Safer and lighter vehicles (based on materials and electronics)	$ 70 billion per year
Energy (Sustainability)	- Reduction in energy use	$ 100 billion per year (on savings)

Over the years, our group had the opportunity to contribute to nanotechnological advances in multiple areas, i.e., electro-optics (optoelectronics and photonics), energy production and mass separation systems and involving membrane and nanocomposite technologies, nano-electromechanical systems (NEMS) for electronic applications, biomedical device applications, to name the most effective ones. Thereby our focus has been to identify the origin for “exotic” material behavior, and to provide physical parameters to cognitively tailor synthesis efforts and/or manufacturing process parameters towards material and device engineering. Our efforts have been predominantly centered around organic materials, as they can be tailored with nearly endless variations in chemical structures opposed to inorganic materials that are mostly limited to elemental compositions.

In this section, some of our efforts will summarized that are related to electro-optics, membrane technologies, and a NEMS application towards thermomechanical ultrahigh density digital storage.

4.1 Electro-Optics

In this subsection, I will discuss our involvements regarding two device technologies in electro-optics (optoelectronics and photonics) with focus on organic/polymeric materials. In regards of optoelectronics, I will address how interfacial constraints can be utilized to increase the device efficiency, and how early molecular mobility assessment of the material can provide important optimization parameters for the device manufacturing process. Furthermore, I will summarize our group's contribution in regards of organic NLO materials for photonic applications. Thereby, I will attend to current challenges in regards of device efficiency and stability, and offer solutions based on our group's involvement in molecular scale thermomechanical analysis.

4.1.1 Organic Optoelectronics

Over the past decade, material synthesis of novel light emitting polymers have made amorphous, disordered organic semiconducting materials interesting as an attractive alternative to state-of-the art inorganic materials used in light emitting diodes (LED). Polymers are attractive because of their mechanical properties. They can be easily shaped in any form, and their processing steps are fewer, and offer improved economical solutions than current device fabrications. Often, they exhibit unique properties, which present additional opportunities for exploration. For instance, polymers systems involving interfacial constraints, such as blends, have shown superior properties, such as more efficient energy transfer, or enhanced electroluminescence and lasing. We have focused in our research on two aspects: (i) the enhancement of LED efficiency based on interfacial constraints, and (ii) the development of material screening methodologies that provide step-by-step insight in the course of the manufacturing process to identify optimized process parameters.

(i) Interfacial enhancement of LED material efficiency: Polymer and organic LED devices involve thin films, on the order of 10 to 100 nm thickness, often in form of a single or two-layer structures that are sandwiched between two electrodes. It was found that in polymer systems, interfacial confinement effects are noticeable over distances of tens to hundreds of nanometers.[11] An example is the LED device performance in intensity and emission color that is strongly affected by interfacial constraints.[11]

The interfacial confinement aspect shall here be illustrated with our study of poly(9,9-dioctylfluorene) (PFO) a promising blue light emitting LED diode material.[41] Polyfluorenes are of great commercial interest for display applications because of their blue color emission, high photoluminescence yield in the solid state (50%) and good charge transport properties. In dilute non-polar solvent solutions, polyfluorenes exhibit spectrally stable blue light emissions that are assigned to single intrachain excitons. Spin cast into thin films, polyfluorenes exhibit red-shifts, which are attributed to aggregate emissions in the solid state. Also, PFO tends to crystallize due to its rod-like molecular configuration, resulting in an undesired red shift in the photoluminescence (PL) signal, and reduced PL efficiency. To hinder crystallization, we investigated in PFO interfacial constraints towards suppressing molecular mobility.

Figure 4-1 illustrates interfacial constraints that take effect in PFO below a film thickness of ~50 nm. T_g was found to increase by 10 °C at a film thickness of 30 nm compared to the bulk, Fig. 4-1(*Left*). As an increase in T_g originates from a conformational change in the polymer, it can be expected that the optical properties are affected. This is confirmed with Figure 4-1 (*Right*), which reveals an altered photoluminescent spectrum for a 30 nm thick film compared to the bulk. Both the thick (187 nm) bulk film, and the thin-confined film show well-structured, vibronic peaks. The first peak (437nm), the second peak (463nm), and the third peak (493 nm) correspond to singlet exciton decay and are indicative of 0-0, 0-1, and 0-2 vibronic transitions, respectively, between the lowest levels of the first excited state to various vibronic levels of the ground state.

According to a study by Winokur *et. al*. (*Phys. Rev. B* (2003), **67** 184106), PFO or other conjugated polymers are, in general, neither homogeneous nor in equilibrium. At room temperature, PFO exhibits primarily a β conformation, i.e. ordered phase. The order-disorder

transition (ODT) is known to take place about 5 to 10 °C above the glass transition temperature. Winokur *et. al*. also found that the emission from 0-0 and 0-1 bands are due to residual α conformation region of the polymer, i.e. the system is a mixture of the ordered β phase with patches of the disorder α phases. Thus, based on the PL spectrum (Fig. 4-1) the 30 nm PFO films contains more of the α phase, while the 187 nm PFO films contain more of the β phase. This led us, considering the thickness dependence of T_g, to conclude that the interfacial constraint in the 30 nm film depressed crystallization, and thus, inhibits the shift of the photoluminescent spectra to longer wavelengths due to intrachain excitons.

This study illustrates how molecular mobility, and, by extension, optical properties can be controlled by introducing dimensional constraints to optoelectronic polymeric systems.

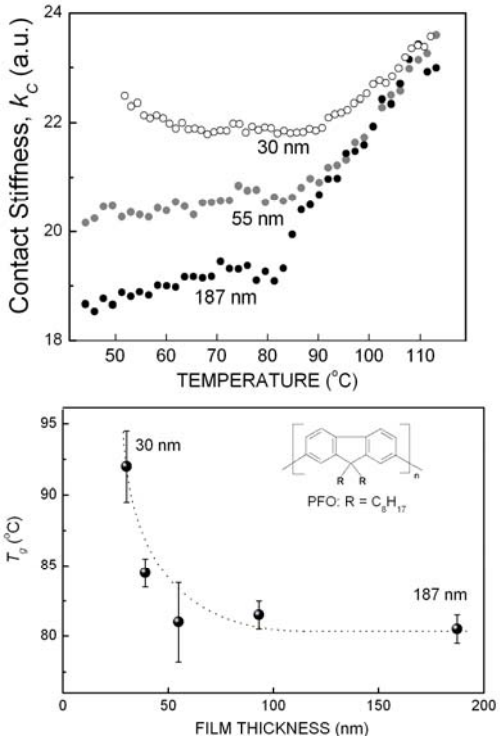

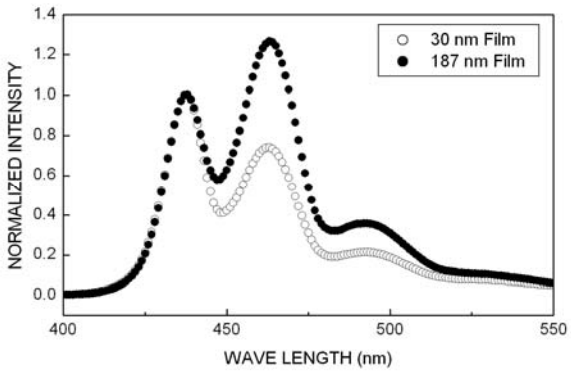

Fig. 4-1: (*Left-top*) SM-FM transition analysis of PFO as function of the film thickness. The shifts in the SM-FM kinks reveal a shift towards higher glass transition temperatures for thinner films. (*Left-bottom*) Film thickness dependence of glass transition temperature on PFO films. (*Right*) The photoluminescent spectrum of the PFO films reveals with the depression of the longer wave length peaks in a 30 nm film compared to a 187 nm film improved spectral stability.

(ii) Optimization of LED manufacturing conditions based on early material analysis *vs.* complex device analysis: An inherit problems with LED materials, i.e., conjugated polymers, is their poor solubility in common organic solvents that prevents them to be easily processed into high quality thin films. One approach to circumvent this problem is the use of solution-processible precursor polymers that can be converted into active polymers. For instance, the precursor for poly(*p*-phenylenevinylene) (PPV), one of the most widely used and researched organic LED polymers, is the PPV sulfonium precursor. The thermal conversion process into PPV is illustrated in Fig. 4-2.

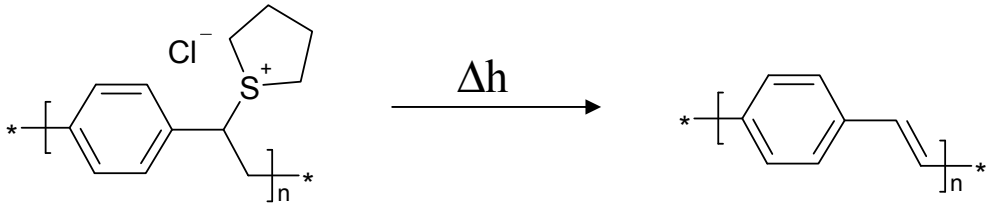

Figure 4-2: Thermal conversion of PPV from its sulfonium precursor.[42]

Problems with the post-casting conversion are, however, the generation of by-products, such as the formation of carbonyl groups (via oxidation), and residues of precursors, which require careful consideration concerning the conversion conditions, as they are one of the origin for a reduced electroluminescent efficiency.

Post-casting conversion generally causes smaller sized molecules that exhibit higher mobility, and are found predominantly at the interface. Thus, we studied the near surface glass transition process for thick (~ 100 nm) PPV sulfonium precursor films containing tetrahydrothiophenium (THT) leaving groups after they were converted into PPV for a range of conversion temperatures.[42] Near surface glass transition values, as determined in by SM-FM, Fig. 4.3(a), were determined as a function of the conversion temperature, T_{conv}. Figure 4-3(b) shows that the T_g relaxation process is strongly conversion temperature dependent. Thereby, the magnitude of the transition value is measure of the molecular mobility. In a system that is not well equilibrated, such as spun-cast, thin films of "bulky" polymers, an increase in molecular mobility can lead to enhanced but undesired conformational changes in the polymer matrix (e.g., π-stacking).[42] Such conformational changes can result, for instance, in the loss of the spectral stability, or in other words, in a decrease of the PL efficiency.[42]

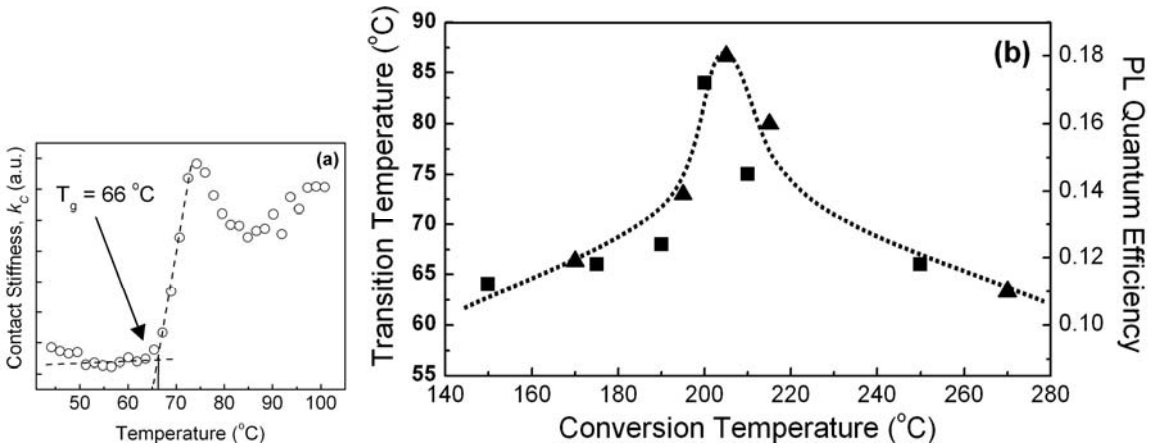

Fig. 4-3: (a) Representative thermal-rheological SM-SFM plot of PPV at a conversion temperature, T_{conv}, of 175 °C. (b) Qualitative comparison of the photo-luminescence (PL) efficiency (▲) with the rheological transition (■) as function of the PPV conversion temperature. The rheological transitions were measured with the SM-FM method. A dashed line has been added for trend enhancement.[42]

We superimposed the transition data in Figure 4-3(b) with the PL efficiency, and found as expected a striking qualitative resemblance of the two data sets, if plotted as function of the conversion temperature. The optimum PL efficiency and maximum glass transition value, obtained at around 205 °C, divides the data set into two regimes.

In the lower temperature regime (T_{conv} < 205 °C), we argued that incomplete PPV conversion is responsible for a low PL efficiency.[42] Unconverted polymer chains shorten the conjugation length, leading to reduced PL efficiency. At the same time, the residual byproduct from the conversion reaction acts as a quenching site through a heavy atom mechanism (spin-orbit coupling between exciton and sulfur atom), which in turn negatively impacts the PL efficiency. It should be noted that the PPV conversion is complete in the bulk system at around 160 °C.

The rheological data suggest that with increasing conversion (thus, PL efficiency), significant conformational changes occur in the material. This is similar to findings that significant geometrical rearrangements are required for the polymer chains to achieve a delocalized conjugated segment. The π-delocalization over adjacent aromatic rings, which increases the conjugation length and segmental stiffness, increases the activation energy for the T_g relaxation process. The degree of molecular rearrangement as function of the conversion temperature is

also noticeable in the measured film thickness, Fig. 4-4.[42] The thickness is found to steadily increase with T_{conv} in the lower temperature regime.

In the upper temperature regime (T_{conv} > 205°C), oxidative degradation processes, such as the formation of carbonyl groups, and aggregation processes due to crystallization reduce the PL efficiency.[42] Since oxidative degradation occurs by breaking the vinylene π bond, the flexibility of the backbone chains is consequently increased. This increase in flexibility is known to decrease the value of T_g. Thus, the decrease in T_g with increasing T_{conv} above 205 °C can be interpreted as enhanced oxidation in the film. The thickness-conversion temperature plot in Figure 4-4 suggests that in the upper conversion temperature regime, significant reorganizations in the film occur that can be attributed to crystallization, which in turn depresses the PL efficiency.

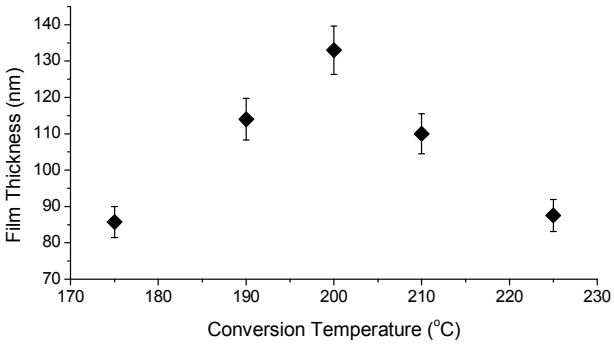

Fig. 4-4: PPV film thickness as a function of the conversion temperature determined by profilometry.

What is particular appealing concerning this study is that the PL efficiency can be pre-assessed for a system, which in its final "sandwiched" device form is very difficult to analyze. Such a pre-assessment is desirable, as additional complications involving the electrodes and interfacial transport resistances can be excluded, and analyzed later independently. That indeed nanoscale thermomechanical property analyses predict a variety of transport phenomena has been a repeating and promising scheme of our research. In the next subsection, this notion will be further emphasized with another technological example, this time it is situated in photonics.

4.1.2 Photonics

Organic based NLO materials for photonic applications have been of interest due to their superior electro-optic (EO) properties, the mechanical and processing advantages of organically synthesized materials, and most importantly, because of the tunability of their EO properties upon molecular design. Recent advances in the design of chromophores guided by theoretical descriptions of structure-function relationships has enhanced non-linearity by more than two orders of magnitude.[3,6,10,43] In the pursuit of highly efficient electro-optic photonic materials, however, one struggles with translating high molecular non-linearities, involving dipole moment carrying chromophores, into large macroscopic EO activities.[3,6,10,43] Currently, our efforts are directed towards the generation of stable assembly of acentrically ordered chromophores within an organic matrix based on cognitive molecular design approaches. The challenges we deal with are as follows:

Highly dipolar chromophores are susceptible to undesirable aggregation that originates from the anisotropic rod-like molecular shape of the chromophores and their strong electrostatic interaction forces. An apparent solution to reduce chromophore aggregation is to lower the loading density of the chromophores, which in turn, however, moderates the EO activity. A possible way out of this dilemma, and a way to achieve a high loading density with minimal chromophore aggregation, is the "site-isolation" approach, where bulky constituents, e.g. dendrimers, are grafted to the chromophores, as illustrated in Fig. 4-5(a).[6,10] The dendrimers act as chromophore cages thereby screening the electrostatic forces and shifting the overall shape of the chromophores from an anisotropic rod-like shape to a more spherical one. We explored this approach experimentally and theoretically for a variety of systems with positive results.[4,6,10] Another approach to reduce dipole annihilation with high chromophore density involves self-assembled EO molecular glasses through strong phenyl-perfluorophenyl (Ph-Ph^F) π–π interactions to improve poling efficiency and chromophore alignment stability, Fig. 4-5(b).[3,4] This novel class of EO materials resulted in EO coefficients exceeding those reported for NLO polymers, Fig. 1-8, as discussed in subsection 1.1 (Fig.1-4).

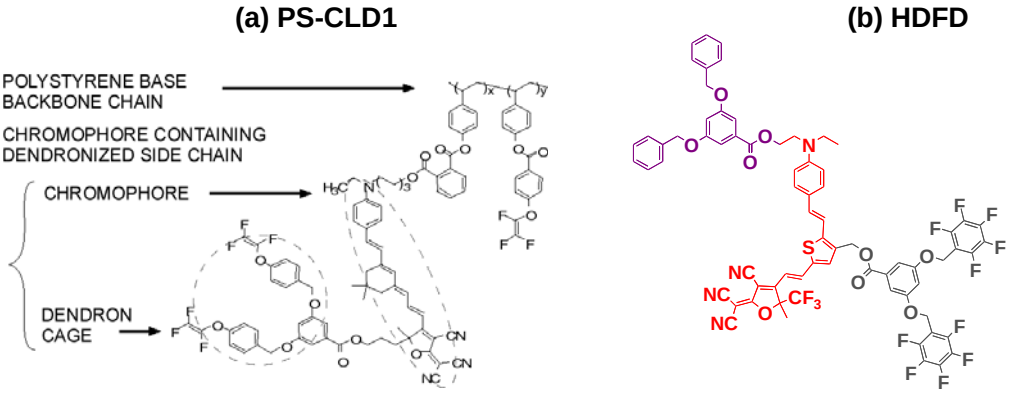

Fig. 4-5: (a) Dendronized side-chain EO polymer, PS-CLD1.[4,6,10] The dendron moiety is attached to the chromophore containing side chain that is connected to the polystyrene-base backbone. (b) Glass forming chromophore containing molecule with phenyl and pentafluorophenyl rings incorporated as peripheral dendrons on the π-bridge and the donor-end of the chromophores, HDFD.[3,4,43]

An important problem still in need of a solution is the development of an effective field poling process of NLO materials, and the production of high non-linearity with long term stability of acentric order. This problem is generally only addressed by trial-and-error approaches. To approach the problem from a guided fundamental perspective demands knowledge about inter- and intra-molecular mobilities of the complex condensed organic EO materials systems.

The general theme in designing chromophore NLO polymer systems has been to increase the glass transition temperature, thus reducing the mobility of the chromophore moiety. However, this approach also reduces the poling efficiency, due to hindered molecular mobility. Thus, what seemed to be at first sight a suitable approach demands a high degree of delicacy, and, a more subtle approach to achieving mobility has to be taken. While there are many cross-linking approaches reported in the literature, most contain obvious deficiencies. For example, thermoset cross-linking processes are triggered under poling conditions, which hardens the matrix while poling is still in progress. As a result, the EO activity is lowered. Ideally, the poling process should be separated from and followed by the cross-linking process. Moreover, to maintain the achieved polar order of the resulting chromophore alignment, the cross-linking reaction should be triggered only under very mild conditions, preferably without further temperature elevation. To accommodate these requirements, we are currently also investigating NLO side-chain chromophore systems with delayed crosslinking abilities based a reversible Diels-Alder cycloaddition reaction, integrated into a chromone-type chromophore side-chain NLO polymer (Jen, Macromolecules **37**, 688-90 (2004)). This approach provides high mobility NLO solid state organic material with excellent solubility for spin casting, and improved thermal stability of the poled order.

Considering the complex molecular NLO building blocks described above, and the desire to locally control the orientation of the chromophore subunits, we employed novel microscopic tools and methodologies, i.e., SM-FM and IFA, as described above in subsection 2.2 and throughout section 1, respectively. We used these tools towards direct investigation of available relaxation processes within the organic matrix (see Fig. 1-1 and Fig. 1-3), their activation energies (see Figs 1-5 and 1-10) and their cooperative phenomena (see Figs 1-5 and 1-10). As discussed previously, dendronized side-chain EO polymers, such as PS-CLD1, and self-assembling NLO molecular glasses (e.g., HDFD) revealed temperature windows bordered by distinct submolecular relaxations appropriate and necessary for effective acentric poling. Energy determinations involving IFA revealed the submolecular origin of relaxation processes, and thus, valuable input for the synthetic design for the next generation of organic NLO materials. In consequence, SM-FM and IFA has proven to be a viable alternative to the current trial-and-error approaches. That chemical synthesis can indeed profit from experiments as described above and yield superior

acentrically ordered NLO materials with higher EO activity was illuminated with an example in Figure 1.2 and a discussion in subsection 1.1.

The electro-optical research, summarized here, considered two distinct approaches for material manipulation. While in optoelectronics interfacial constraints were used to increase the device efficiency, in photonics, intra- and intermolecular constraints were employed. With the study of the conversion process in conjugated polymers, a methodology was introduced that provides a pre-assessment of the electronic transport properties on a step-by-step basis during the device manufacturing process. That indeed also mass transport properties can be pre-assessed with local thermomechanical analyses is addressed in the next subsection.

4.2 Membrane Technology

Thinking of heterogeneous membranes and mass transfer there are two major constraints that come to mind: (i) The constrained motion of molecules through membranes, and (ii) material constraints within the membranes imposed by material heterogeneities and the presence of interfaces. In this regards, our past and current research interest has been focusing on two polymer transport systems: (a) Polymer electrolyte membranes (PEM) that are known for their complex heterogeneous internal structure, and (b) nanocomposite membranes with imposed interfaces. Here, I will summarize our efforts on water transport through PEM Nafion® and reverse selective nanocomposite membranes involving stiff, and high free-volume conjugated polymers.

4.2.1 PEM Fuel Cell

To date, the most widely used polymer electrolyte membrane (PEM) material in fuel cell application is Nafion®, an ionic copolymer (ionomer). It consists of a poly(tetrafluoroethylene) backbone with short perfluoro-polyether pendant side chains terminated by ionizable sulfonate groups, as depicted in Figure 4-6. A complex organized structure, when swollen in a polar solvent (water or alcohols), is responsible for excellent ionic conductivity and electrochemical and chemical resistance. Our current understanding of the Nafion structure is that it resembles a three dimensional array of inverse micelles that are interconnected by short channels acting as transient crosslinks. The micelles, 30 to 50 Ångstrom in size, consist of ionic end groups from the side chains that are clustered together in solvent-containing aggregates within the apolar perfluorocarbon matrix.

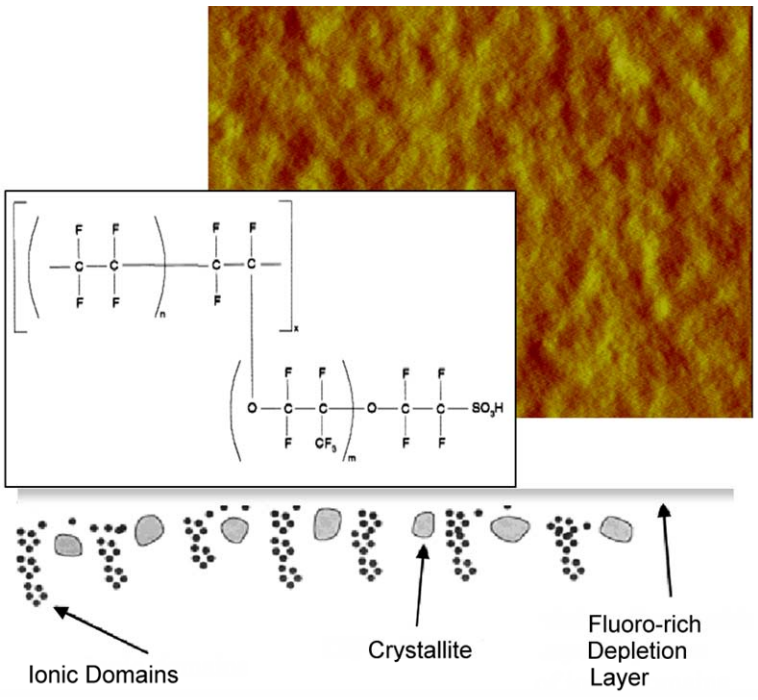

Fig. 4-6: PEM Nafion®: Chemical Structure, cartoon of condensed phase with ionic domains, imaged by AFM (300 nm horizontal scan).

Nafion membranes are rigid systems with poor proton conduction unless a polar solvent is absorbed. For insufficiently hydrated Nafion membranes, the proton transport is slow, and thus, the conversion efficiency negatively affected. On the other hand, excess water can lead to cathode flooding in the system, resulting in a reduced efficiency. Good water management usually requires balancing the electro-osmotic drag and diffusion of water. It has been realized that the microstructural properties of

the membrane are very important in explaining solvent swelling.

Besides water transport, the gas permeability, in particular of oxygen and hydrogen, is of significance for an effective PEM membrane operation. Originally, it was argued that the gas permeation is mainly either through the hydrated ionic cluster region, or through the hydrophobic amorphous region of the membrane. Recent experiments, however, showed that both regions have to be considered for gas transport.

Over the past decades, the main research focus has been on the solvent swollen membrane. It was found that a decrease in resistivity around 80-90 ^{o}C is due to a reduction in the activation barriers for proton motion, which is generally attributed to the availability of water to ionize the sulfonic acid groups. Considering the complexity of Nafion that intertwines a rheological polymer cluster network with the intricacy of solvent swelling and ionic conductivity, it is desirable to investigate gas transport and swelling in conjunction with the rheological relaxation properties of the polymer matrix.

We approached this problem first with an SM-FM thermo- mechanical transition analysis applied to non-dehydrated membranes, Fig. 4 7.[44] A structural transition at 79 ^{o}C, about 30 to 40 ^{o}C below the glass transition temperature of Nafion (H^{+} form), was found for the dehydrated membrane. To directly connect this low temperature transition to the membrane's transport ability of water, we had to device an instrumental approach that is sensitive enough.

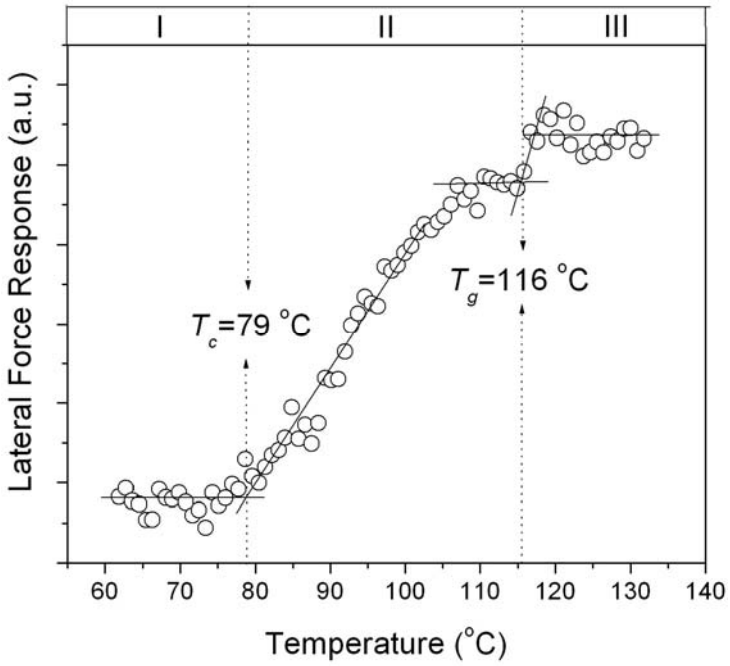

Fig. 4-7: SM-FM analysis of dehydrated Nafion (EW of 1100). Shear response forces reveal two transition temperatures that identify three regimes. Regime I and III reflect the glass state and the rubber melt state of Nafion, respectively. Regime II encompasses the creep regime over which the cantilever sinks into the polymer matrix to equilibrate the contact pressure, and the saturation regime that defines the phase between the glass and rubber states.[44]

Considering the intricacy between locally constrained membrane properties, and the selective permeation of analytes and solutes through porous and non-porous, organic and inorganic, heterogeneous systems, it is perceivable to look for a probe that provides *in-situ* microscopic information about the local permeability. Naturally, scanning force microscopy (in particular, lateral force microscopy LFM) comes to mind. Not unlike the principle of an air-hockey table, where the puck experiences the air cushion as a friction reducing medium, it can be imagined that a LFM cantilever sliding over a membrane that is penetrated by a fluid is subjected to "lubrication". This brought forward the development of flux-lateral force microscopy (F-LFM), as illustrated in Fig. 4-8.[44]

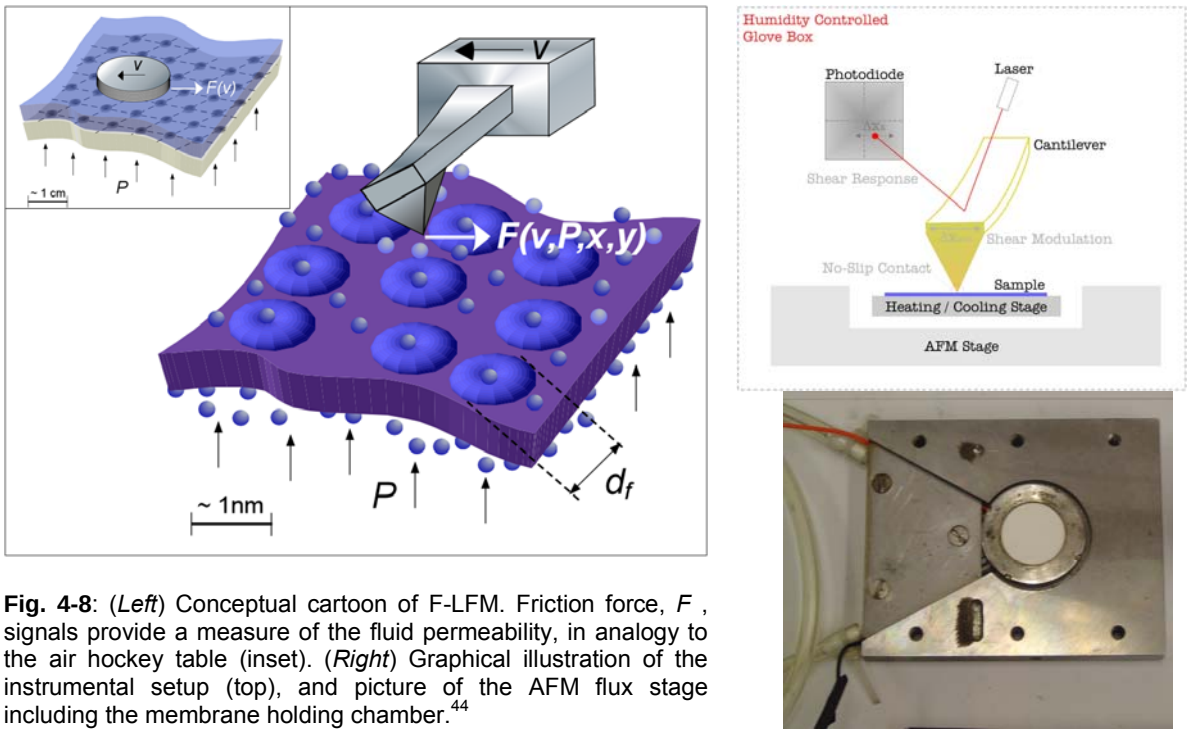

Fig. 4-8: (*Left*) Conceptual cartoon of F-LFM. Friction force, F , signals provide a measure of the fluid permeability, in analogy to the air hockey table (inset). (*Right*) Graphical illustration of the instrumental setup (top), and picture of the AFM flux stage including the membrane holding chamber.[44]

Our in–house developed F-LFM technique was calibrated with MFI zeolite membranes (micropore sizes of ~0.5 nm) of known macroscopically determined N_2 permeabilities. From linear lateral force *vs.* permeate inlet pressure plots (FP plots), Fig. 4-9, we deduced the membrane specific FP gradients, and found them to be proportional to the measured N_2 permeabilities of three zeolite standard membranes. This result indicated that FP gradients offer a direct measure of nanoscale permeabilities.[44]

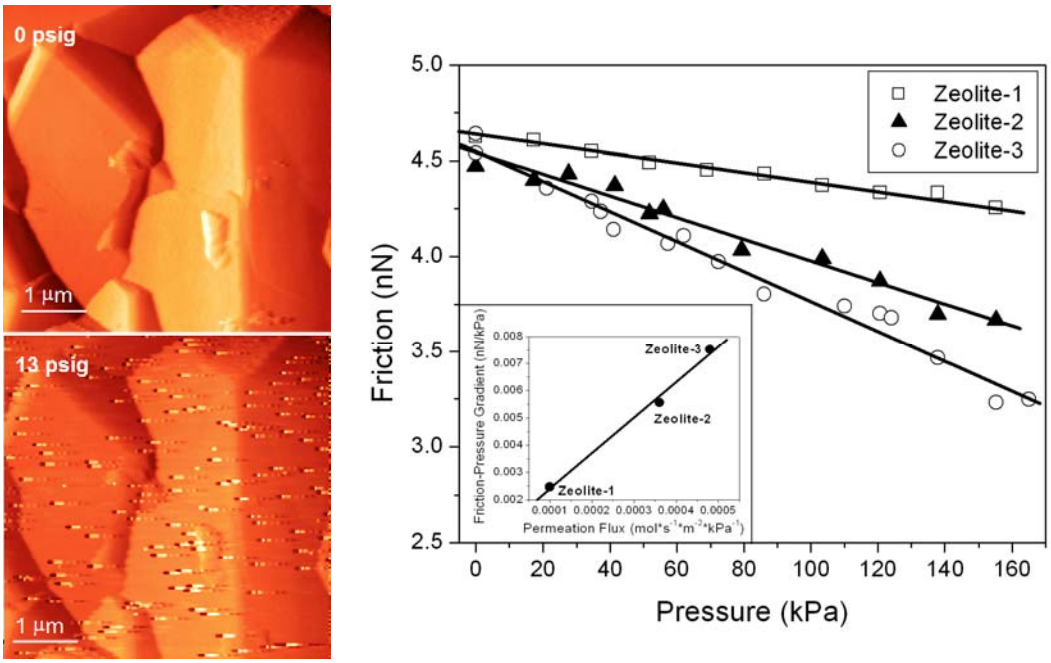

Fig. 4-9: MFI zeolite membranes. (*Left*) AFM images illustrate the importance of membrane purging prior to F-LFM analysis due to organic due to possible organic contamination (bottom). (*Right*) F-LFM analysis reveals direct linear correspondence between FP gradients and macroscopic permeation fluxes.

With F-LFM, we explored the impact of the structural reorganization at 79 °C on water transport in a commercial Nafion 115 PEM membrane. The membrane was placed onto the airtight membrane holding chamber, Fig. 4-8, through which it was exposed to a hydrated nitrogen gas on the upstream side. The downstream side of the membrane, kept dry by a nitrogen < 10% RH nitrogen environment, was probed by a cantilever tip at a constant sliding velocity. The results of this study are presented in Figure 4-10. It provides the first direct observation of water transport through a Nafion membrane. Up to a temperature of 70 °C, the *FP gradients* increase steadily, as found for the permeability of nitrogen through Nafion. Between 70 °C and the low-temperature matrix relaxation at 79 °C two distinct signal responses occur in the *FP gradient* plots, highlighted in Figure 4-10(b), one belonging to the nitrogen transport and the other one to water transport. Above 79 °C, the sign of the *FP gradients is* reversed, indicating that the friction force increases with pressure. In this regime, the cantilever experiences a water-swollen membrane with masked nitrogen transport and dominant water transport. In contrast to the "incompliant" zeolite membrane, the Nafion polymer membrane is elastically and plastically deformed by the tip, which exerts pressures in the contact zone on the order of 100 MPa. Particularly plastic deformations can dominate any other source of frictional dissipation. Thus, as the qualitative behavior of *FP gradients* below 79 °C is a direct consequence of nitrogen and water permeation, above 79 °C, it is dominated by the deformation properties of the swollen Nafion membrane. Based on our study it can be concluded that a structural transition at 79 °C within the Nafion matrix is responsible for sufficient water transport. It explains the poor performance of Nafion membranes below ~80 °C, as water, the osmotic transport system for the protons, is trapped within the membrane. Future research, involving for instance IFA, is necessary to provide molecular scale insight into the transition process at 79 °C. It can be expected that the structural relaxation affects the ionic clusters, and thus, opens up a gateway for water to diffuse.

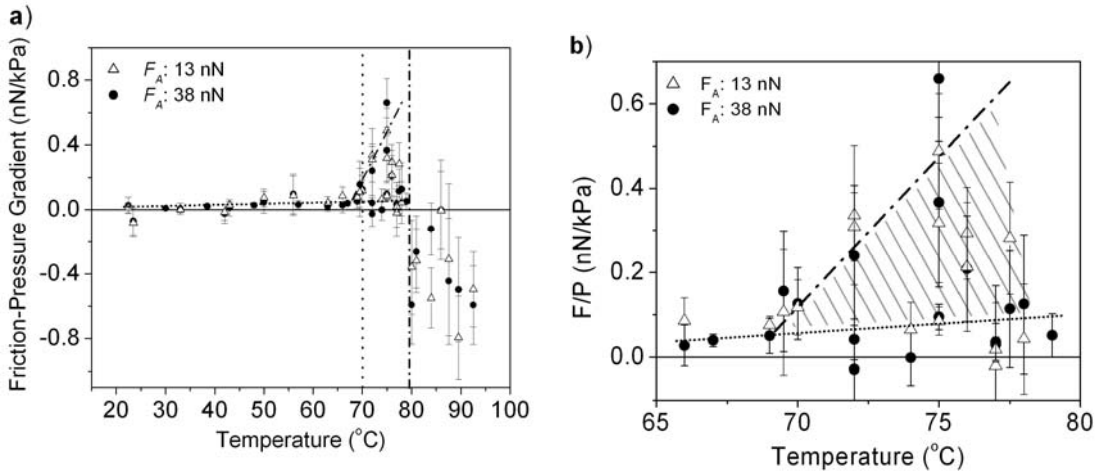

Fig. 4-10: F-LFM measurements Nafion 115 PEM membrane.[44] (a) FP-gradient analysis at an applied load of 13 nN (triangle) and 38 nN (dot). The regime up to the vertical dashed line at 70 °C reflects an increase in the nitrogen flux (visually enhanced by the dotted trend line). Nominally increased fluxes are observed above 70 °C, and below the low temperature matrix relaxation of dehydrated Nafion at 79 °C (indicated by the second vertical dashed line). Above the 79 °C mark, the force pressure gradient is reversed, reflecting the changes of the water-swollen PEM membrane. (b) Zoom into the transition region (dashed area) where the onset of water transport is recognizable. Water and nitrogen transport are occurring simultaneously as indicated by the dashed lines. Two distinct signal responses occur in between 70 °C to 79 °C indicative of the two transports of nitrogen (dotted line) water (dotted-dashed line).

Besides providing fundamental insight into material and transport properties of complex and constrained material our group is also involved in device developments. That shall here be briefly

illustrated concerning an ultrathin design of a PEM fuel cell device using a soft lithographical technique involving poly(dimethyl-siloxane) PDMS.

The target of our design have been the generation of flow field plates with micro-channels (see Fig. 4-11) This design was motivated by the desire

(i) to slow down the flow velocity of the fluids within the flow field plates with dimensional constraints, which results in an increase in the "fuel" efficiency,
(ii) to lower the manufacturing process by avoiding the expensive graphite flow field plates, and
(iii) to provide mechanical flexibility to the fuel for multiple reasons.

A very costly component in PEM fuel cell stacks is the bipolar/end flow field plates. They account for more than 80 % of the total weight, and are very expensive to manufacture. Currently, the flow field channels are machined or molded into bipolar plates of graphite or compression molded blanks of filled poly(vinylidene fluoride) (PVDC) polymers. A cost alternative to graphite is compression molded thermoset plates with molded-in channels, which cost only one-fifth compared to graphite. Channel flow analyses (Kumar et al. (2003) J. Power Source) indicate that a decrease in the channel width that results in an increase in the pressure drop is improving the fuel cell performance, as it shifts the transfer process type of the reactant gases towards the electrode-membrane reaction interface from diffusion to forced convection.

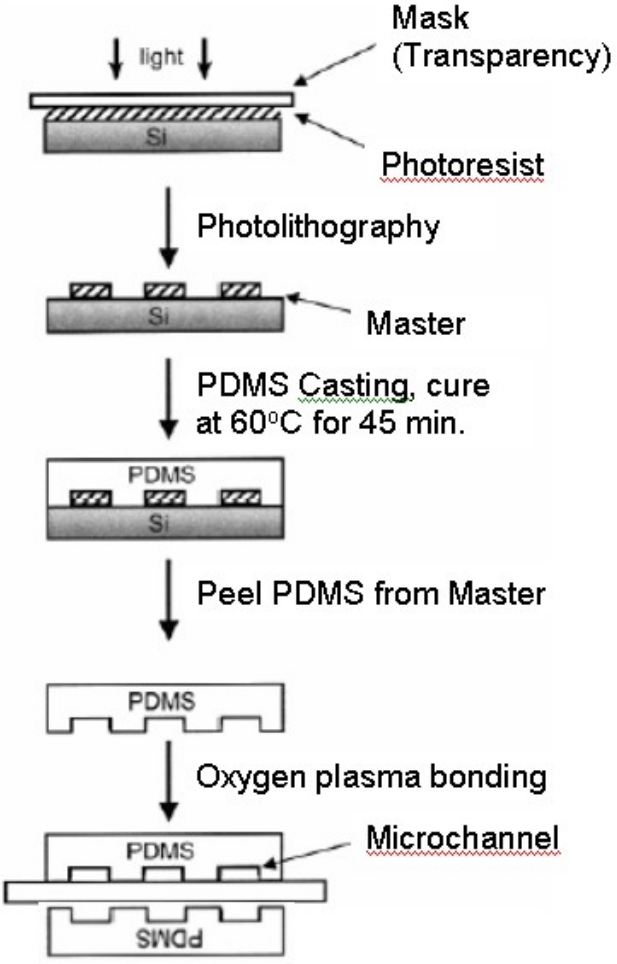

Fig 4-11: Fabrication (soft lithograph) of the PDMS Flow Field Plate.

As illustrated in Fig. 4-12(*Left*), the flexible membrane electrode assembly (MEA) containing the PEM membrane is sandwiched between the flow field plates in state-of-the art PEM fuel cells. The bulky (non-flexible and heavy) parts are the graphite based flow field plates. With soft-lithography, as described in Figure 4-11, involving flow field masks of the sort presented in Fig. 4-12(*Left*) with microscale dimensions of flow channels, we fabricated a flexible fuel cell device, Fig. 4-12(*Right*). First studies showed good flow performance. On-going work focuses on involving material such as PVDC for actual fuel cell operation.

Thus, while our group's research and engineering involvement in fuel cell applications, has focused on establishing an understanding of the internal complexity within a complex polyelectrolyte membrane system and its impact on mass and consequently electric transport properties, our research effort described in the following subsection is attentive to mass transport in interfacially constraints systems. Our specific attention is on reverse selective transport in nanocomposite polymer membranes.

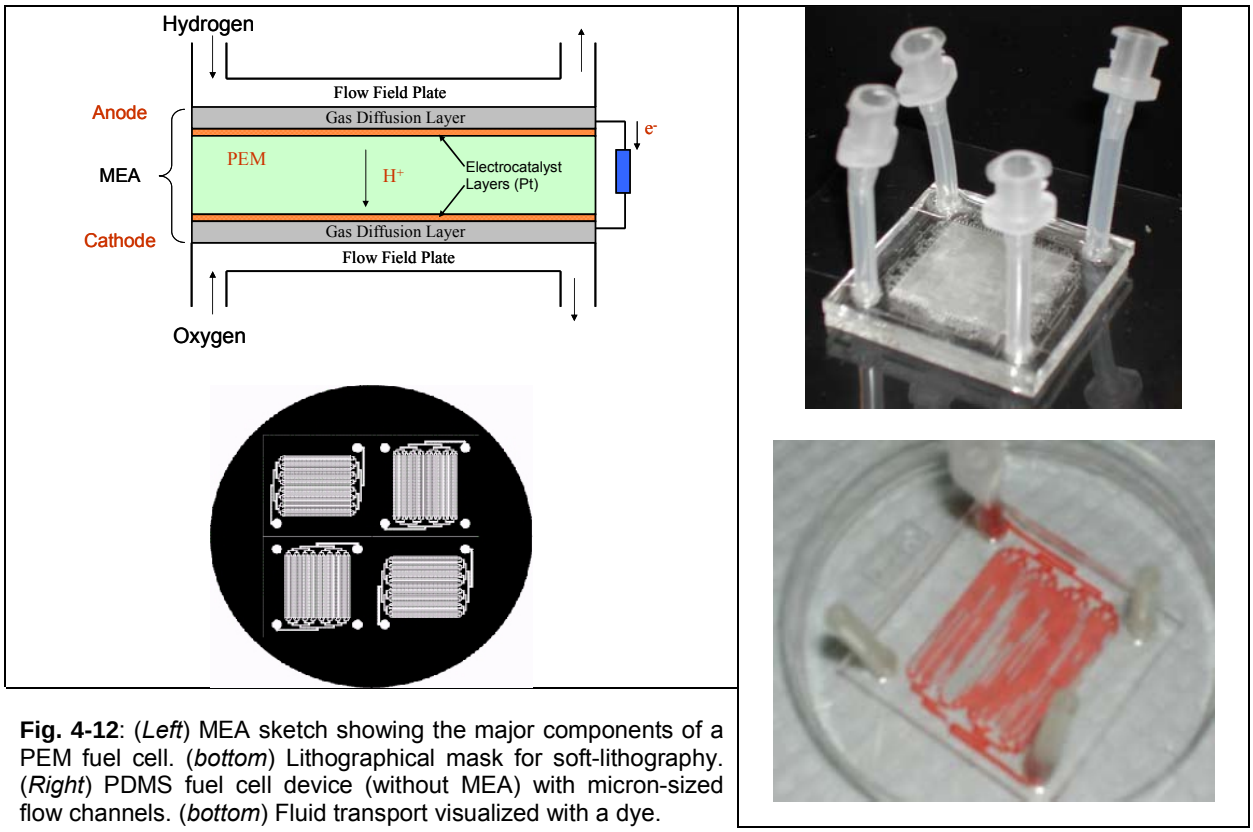

Fig. 4-12: (*Left*) MEA sketch showing the major components of a PEM fuel cell. (*bottom*) Lithographical mask for soft-lithography. (*Right*) PDMS fuel cell device (without MEA) with micron-sized flow channels. (*bottom*) Fluid transport visualized with a dye.

4.2.2 Nanocomposite Membranes

Of particular interest to the chemical processing industry are reverse-selective membranes (also called solubility-selective or vapor-selective), which can be used for separating larger organic molecules from smaller permanent gases. These membranes find numerous chemical and refining industry applications including removal of higher hydrocarbons from methane, olefin separation from nitrogen, and removal of hydrogen from refinery process gas streams.

While the pore-transport model can be used to understand transport in high free volume glassy polymers, the solution-diffusion model is more generally applied. According to the solution-diffusion model, permeability within a membrane for use in vapor separation can be expressed as the product of the sorption (or solubility) coefficient (*S*) of a penetrant, A, in the membrane times the concentration averaged diffusivity (*D*) of the penetrant through the membrane:[10,32]

$$P_A = S_A \times D_A . \tag{4.1}$$

Sorption in glassy polymers can be understood according to the dual mode sorption model, composed of a combination of dissolution described by Henry's Law and Langmuir surface sorption:[32]

$$S = k_D + \frac{C_H' b}{1 + bp} . \tag{4.2}$$

where k_D is Henry's constant, b is the Langmuir hole affinity parameter, C'_H is the Langmuir capacity parameter and p is the system pressure. Diffusion through membranes is often understood as being primarily a function of free volume, i.e.,

$$D_A = C \exp\left(-\gamma v_A / V_{FV}\right). \tag{4.3}$$

where C and γ are polymer-specific constants, v_A is a critical void volume necessary for the diffusion of A, and V_{FV} is the average void volume of the material. For the separation of multiple

(e.g. two) penetrants, equation (4.1) can be utilized to determine the selectivity, α, of two penetrants, *A* and *B* as:

$$\alpha_{A/B} = \frac{S_A}{S_B} \times \frac{D_A}{D_B}. \qquad (4.4)$$

Smaller molecules generally have higher diffusivities than larger molecules. Thus, when solubility coefficients are similar, the diffusivity ratio (D_A/D_B) dominates in equation (4.4) and selectivity favors smaller molecules (i.e., is size selective). There are, however, polymers where the solubility ratio becomes the dominant term in the determination of selectivity. Included in this group of polymers are: poly(4-methyl-2-pentyne) (PMP) and poly[l-(trimethylsily1)-1-propyne] (PTMSP) and its analogues.[32] These polymers have been shown to exhibit high reverse-selectivity for organic vapor/permanent gas (e.g. n-butane/N_2) mixtures, and high glass transition temperatures, amorphous structures, and extremely high free volumes.

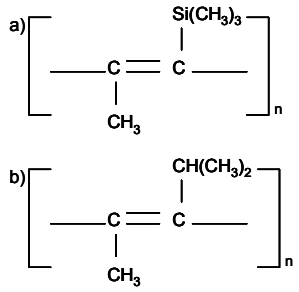

Fig. 4-13: Structures of (a) PTMSP and (b) PMP.

The structures of PTMSP and PMP, depicted in Figure 4-13, show that the polymer backbones contain rigid carbon-carbon double bonds. For PTMSP, bulky trimethylsilyl and methyl constituent groups are also present, which result in very twisted molecules. The twisted conformation in PTMSP is maintained due to the high energetic barriers (40 kcal/mol) to rotation around a backbone single bond. This creates an extremely rigid chain that will maintain conformation achieved during polymerization while changes in chain contour may still occur due to fluctuations in dihedral angles in narrow potential energy wells.

Neat PTMSP (and similar polymers) are understood to have high free volume as a result of the inefficient chain packing of their rigid backbones, bulky pendant groups and poor interchain cohesion. Their free volumes exhibit a bimodal distribution, with sub-nanometer cavities. It has been theorized that these cavities create a series of nanoporous interconnected free volume cavities, thus giving rise to unique high-permeability. This understanding of polymer structure is qualitatively illustrated in Figure 4-14. It is important to note that the polymer system is dynamic, and thus, the channel elements displayed in Figure 4-14 are transient with nanosecond lifetimes. The materials exhibit reverse-selective behavior due to the fact that large organic molecules absorb to the matrix walls within the small free volume elements thereby creating resistance to transport for smaller, permanent gases.

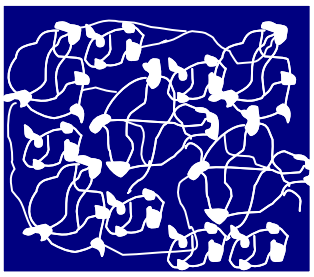

Fig. 4-14: Structure of high free volume glassy polymer

By incorporating fumed silica nanoparticles into the reverse selective membranes, it was found that the permeability and diffusivity of the material is increased. Fumed silica addition had little effect on penetrant solubility, indicating that enhanced diffusivity is primarily responsible for increased permeability. Increases in free volume are thought as origin for improved permeability. Subsequent studies with PTMSP/silica nanocomposites have also confirmed an enhancement in free volume with increasing filler content using both ^{129}Xe NMR spectroscopy (G. Consolati et al. (2006) Polymer Phys) and PALS (A. J. Hill et al. (2005) J. Mol. Structure). A very interesting finding was that at higher silica loadings in PTMSP/FS the permeability of small permeates such as H_2 and methane increased more than the permeability of larger organic vapors such as propane and n-butane.

When fumed silica nanoparticles are incorporated into the polymer matrix the rigid chains are unable to efficiently pack around the particles. This results in a high free volume interfacial region between the polymer and fused silicon particle of low-density polymer that allows gas molecules to diffuse more rapidly, as qualitatively illustrated in Figure 4-15. The morphology of this interfacial region is critical for determining overall transport properties. It has been theorized that conventional solution-diffusion will dominate in the interfacial region as long as void volume

increases do not result in continuous channels. Relatively large continuous channels will allow pore flow transport mechanisms (i.e. Knudsen diffusion) which favor small molecules, resulting in the loss of reverse-selectivity. This phenomenon has been demonstrated experimentally (T.C. Merkel et al, (2003) Macromolecules).

Since the discovery of reverse-selective nanocomposite membranes, much research has been directed toward the study of bulk properties and tailoring them for specific applications. Bulk property improvement through various methods has been achieved by variation of nanoparticle size, variation of bulk filler content and methods for modifying silica particles with functional groups for incorporating nanoparticles into the polymer phase. Although all these property studies have greatly contributed to the understanding of the capabilities of reverse-selective nanocomposite systems, there are still many unresolved key issues, which demand microscopic insight of local variation in the material and transport properties, and more sophisticated processing conditions. The key research issues, our group is focusing on, are obtaining information about local

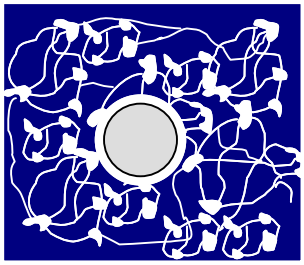

Fig. 4-15: Sketch of membrane structure with single silica nanoparticle.

- impact of interfacial constraints leading to enhanced reverse-selective mass transport,
- effect of the filler particle on polymer material properties,
- experimental confirmation of fundamental interfacial transport models,
- result of filler aggregation on membrane performance, and
- molecular relaxations at the polymer-filler interface that contribute to age susceptibility.

All of these issues are associated with property variations within the nanocomposite membrane and require microscopic probing methods, such as SM-FM, IFA, F-LFM, and heated tip atomic force microscopy (HT-AFM – Fig. 4-16). The objective of our research is to gain basic insight into reverse selective transport by manipulation of filler properties and spacing, with the ultimate goal to develop highly efficient, selective and stable membranes based on fundamentals.

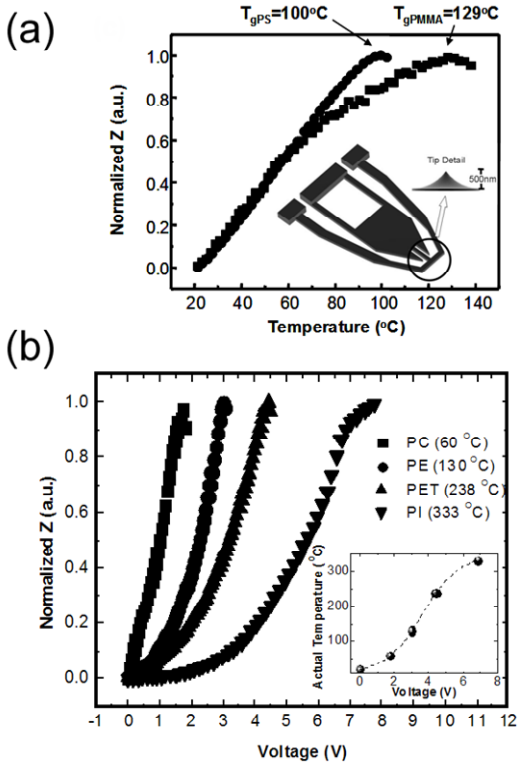

Fig. 4-16: HT-AFM: (a) Lever deflection *vs.* calibrated local temperature.
(b) Temperature calibration based on transition values of calibration standards.

As pointed out throughout this document, tailored nanoscopic tools are paramount for investigating nano-constrained systems. For analyzing the interfacial strength between the nanoparticles and the polymer matrix, we employed heated tip atomic force microscopy towards, a methodology that has been pioneered by our group.[10,32,45] HT-AFM allows for local investigation of interfacial debonding as well as local nano-thermomechanical analysis. *Briefly*: HT-AFM utilizes gradient doped resistive cantilever materials to integrate heating directly into the cantilever probe. Figure 4-16(a), illustrates the complexity of a resistive cantilever, and provides two plots of the cantilever normal deflection signal *Z* as function of the calibrated local temperature (for PS and PMMA). The local temperatures were obtained from calibration plots on a variety of material standards with well known transition values, as documented in Figure 4-16(b). Thereby, the maximum "turning points" in normal

deflection *vs.* cantilever applied voltage plots, Fig. 4-16(b), are equivalent to the glass transition values of the standards.[32] Compared to substrate heating methods such SM-FM, HT-AFM offers some distinct advantages. Foremost is the ability to heat locally to higher temperatures. Other advantages of HT-AFM over global sample heating include the ability to operate at very high heating rates due to the low thermal mass, and the ability to perform multiple measurements on specimens that are highly sensitive to thermal history.

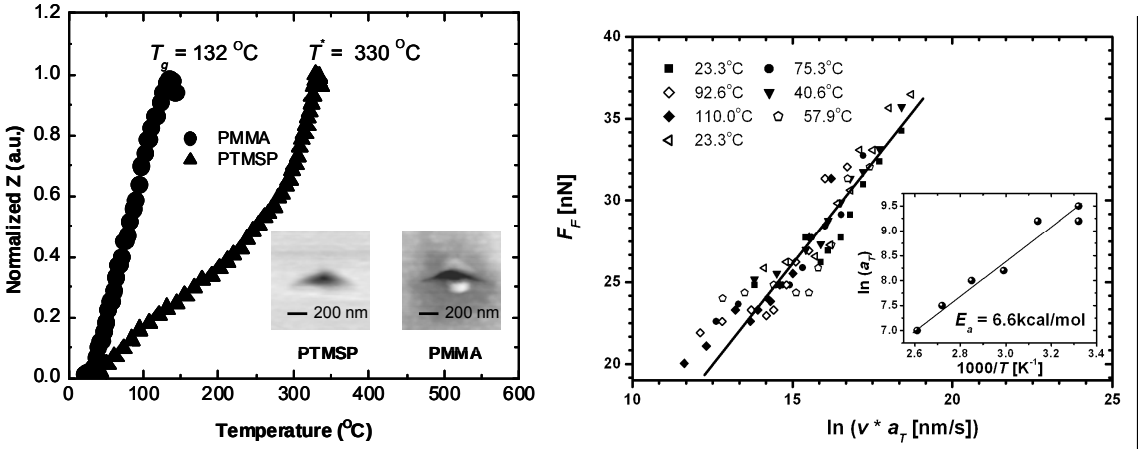

Fig. 4-17: (*Left*). HT-AFM transition analysis for PMMA and PTMSP. The inflection at ~200 °C of PTMPS is indicative of partial degradation. (*Right*) IFA of PTMSP below 110 °C reveals an activated process of 6.6 kcal/mol that is identified as TMS side-chain mobility.[10,32]

Figure 4-17(*Left*) exhibits for PTMSP a HT-AFM transition value T^* of 330 °C. As per our studies, it is indicative of the PTMSP decomposition paired with the glass transition.[32] IFA experiments, Fig. 4-17(*Right*), revealed as the only activated transition process below T^*, the trimethylsilyl (TMS) side-chain rotation around the C-Si bond (see Fig. 4-13).

As for practical applications involving PTMSP membranes, the degradation temperature is avoided in the manufacturing process, the TMS side-chain mobility is of vital significance for the membrane properties. If we consider, for instance, in analogy the side-chain mobility of polystyrene, discussed in subsection 3.1, and its orientational preponderance towards the free surface, it is reasonable to assume that also TMS exhibits an enhanced or reduced presence within the free volume regimes of PTMSP. As there is a noticeable difference in the interaction between the TMS group and monoatomic H_2 and diatomic CO_2, it is reasonable to assume that the TMS contribution towards the relative sorption amount of the two molecules within the free volume of PTMSP is essential. This aspect is currently still under investigation.

Shifting now from neat PTMSP to interfacially constrained nanocomposite PTMSP-fumed silica systems (PTMSP-FS), we can expect as visualized in Figure 4-15, an increase in void spaces. As addressed above, PTMSP-FS is known for its unique improved permeability and reverse selectivity with increased filler concentration up to some level. This behavior however is not unexpected, if we consider our previous discussion. It could be explained by the preferential orientation of the TMS groups in regards of the introduced void space interfaces. Besides a local alteration of the interaction field (some of us would call it “chemistry”), one has however also to consider a physical (phase) change of the polymer matrix towards the composite interface, as discussed in great detail in section 2.

To evaluate the interfacial properties of PTMSP-FS composites, we employed HT-AFM, and investigated the adhesive strength between PTMSP and silica, by controlled debonding of single nanoparticles from the glassy matrix.[32,45] Figure 4-18 reveals that debonding occurs consistently at a temperature tens of degrees below the decomposition temperature of PTMSP. This suggests increased polymer mobility in the interfacial region. The debonding strength was inferred from the torsional bending force of the HT-AFM probe when impacting the particle. With this, HT-AFM has

shown to provide two additional attributes besides of being a thermal transition also to embody a highly sensitive force sensor and a thermomechanical manipulator.

We could also determine the debonding force. It was deduced by integrating the impact peak from onset to peak force, i.e.,[32]

$$E_{db} = \int_{\alpha} \Delta F dx \,. \tag{4.5}$$

where α is the impact duration to peak force, ΔF is the force relative to the baseline friction, and x is the lateral position of the scanner. With this a total debonding energy of 1.5×10^{-5} nJ could be determined. The same experiment conducted with PS and PMMA showed it very difficult (high forces) to remove silica particles from the matrices. As the adhesive forces of PS and PMMA bracket the one of PTMSP, the debonding observations of the three polymers provides the first direct evidence that the actual PTMSP surface coverage of the particles is significantly diminished, due to interfacial void formations as addressed above.

In conclusion, our research on reverse selective polymer membrane materials and nanocomposites revealed the mobility of side chains and the formation of interfacial voids very likely responsible for the unique increase in reverse selectivity and permeability in PTMSP-FS nano-composites. On-going research in our labs involving nuclear magnetic resonance (NMR) experiments and dielectric spectroscopy will provide further insight into the interfacially driven mass transport properties.

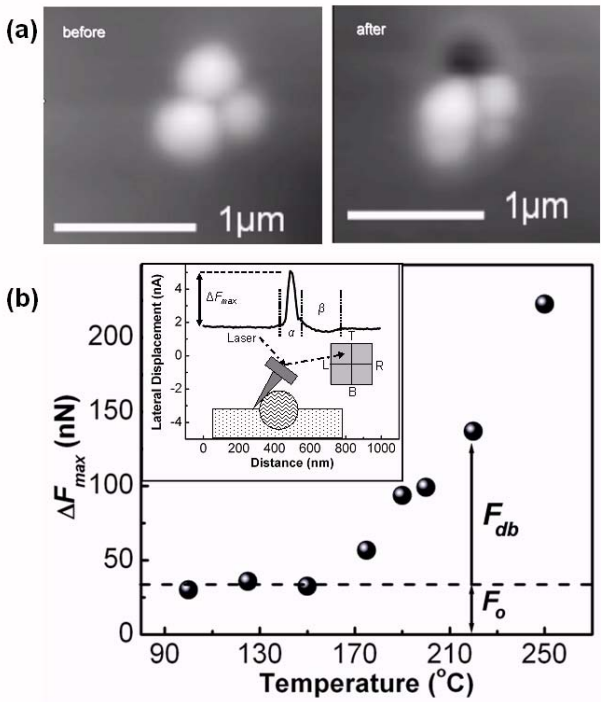

Fig. 4-18: (a) PTMSP-FS nanocomposite images before and after a HT-AFM tip temperature of 250 °C. (b) Lateral impact force ΔF_{max} (see inset) as function of temperature. Debonding occurred above 200 °C. F_o and F_{db} indicate the base force and debonding force, respectively.[45]

4.3 Digital Storage – Thermomechanical Ultrahigh Density Recording

In the previous subsections on technological applications, the focus has been in understanding and influencing transport properties based on constraints in materials. I illustrate here. how also Nanoelectromechanical System (NEMS) processes can benefit from material constraints. The focus is on is ultrahigh density storage by means of nanoindentation.

In section 2, I summarized some of our results concerning interfacial constraints on ultrathin films. In particular in spin cast polymers, we found within the 100 nm boundary region to the substrate a non-linear glass transition profile, as redrawn in Figure 4-19. While analyzing a novel device technology of an ultrahigh density digital storage recording scheme pioneered by IBM, originally named the *Millipede NEMS project*, and today known as *thermomechanical data storage (TDS)*, we realized the importance of the anisotropic interfacial mobility for this application.[29,31] The TDS methodology entails a nanometer sized thermal-indentation bit writing process in ultrathin (~ 30 - 50 nm) polymer films. For films that exceeded the critical thickness δ_{max} at which the glass transition reaches a maximum in the $T_g(\delta)$ profile, we found excessive rims around the TDS bits, while less pronounced rims were detected for $\delta < \delta_{max}$. Our study not only revealed the importance of the local transition property (mobility) towards stress adsorption in the

polymer matrix, but also provided first solutions by tailoring $T_g(\delta)$ profiles accordingly (c.f. sec. 2.2). Our findings[29,31] shall here be a little further reiterated.

The thermomechanical data storage methodology, one of the few true NEMS applications, relies on writing, reading, and erasing nanometer sized data bits in thin polymer films, offering densities up to Tb in^{-2}. In essence, the TDS writing operation is a high speed (MHz), elastic-viscoplastic polymer indentation process, Fig. 4-20, involving on the order of 1000 resistively heated and parallel operated cantilevers. The polymer storage media must be designed to achieve the narrow range of physiochemical properties necessary for: high data density, fast data rates, high durability, long shelf life, and low power consumption. The ideal polymer should be easily deformable for bit writing; however, the written bits must be stable against dewetting, thermal degradation, and wear.

The writing and erasing processes rely on local deformation of the polymer film, and to exploit the enhanced molecular-chain segment mobility above the glass transition point, these processes are conducted at a local temperature above T_g. Elastic recovery of displaced material is prevented by rapidly quenching the indentation site to below T_g, with the probe tip in place. As a result, the deformation is *frozen in* because the motion of molecular-chain segments is effectively inhibited below T_g. In order to preserve the recorded data, any further deformation of the polymer film must be limited during read-back and scanning; therefore, these operations are conducted below T_g, where molecular-chain segmental mobility is effectively inhibited.

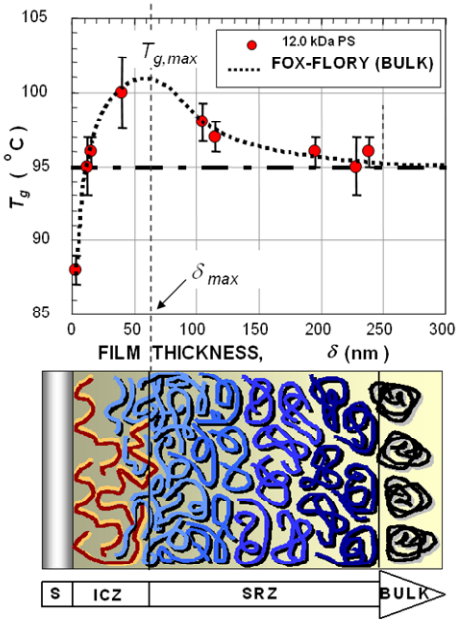

Fig. 4-19: Anisotropic glass transition profile in polystyrene towards a solid silicon surface reveals anisotropy in the material structure and dynamics as sketched.[7]

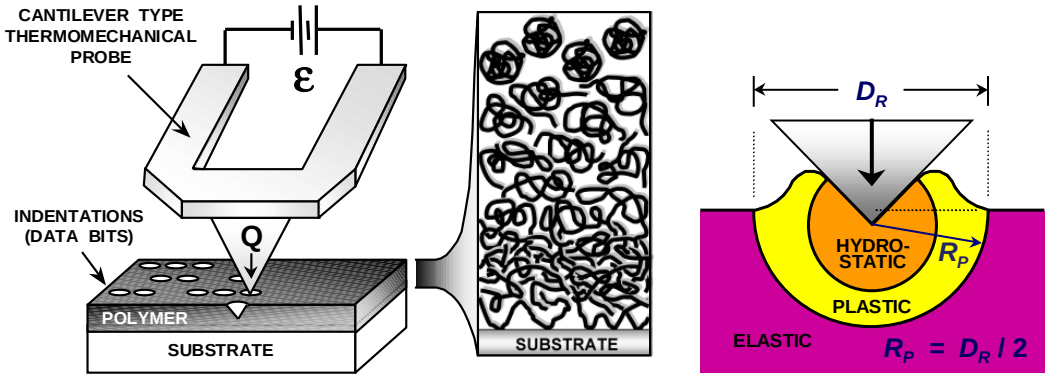

Fig. 4-20: Scanning Probe, Thermomechanical Data Storage: Creating uniform bit indentations in sub-100 nm thick polymer films requires an understanding of the interfacial rheology. (*Left*) TDS illustration with resistively heated cantilever. (*Right*) Illustration of a phenomenolgical matrix deformation model with rim formation.

In addition to achieving the appropriate T_g, the polymer film should exhibit a large drop, by orders of magnitude, in the shear modulus (G) at T_g. When the probe tip is indented into the polymer during writing and erasing (above T_g), the polymer is strained, and elastic shear stresses are incorporated into the film in the vicinity of the indentation. Unlike the deformation of a simple liquid, the indentation represents a metastable state of the deformed volume. The driving force for recovery of the initial unstressed state is directly related to the magnitude of the incorporated

elastic stresses. In the interest of bit stability, elastic recovery should be avoided; hence a low shear modulus, leading to reduced internal stresses during the indentation process (above T_g), is desirable. To further promote longevity of recorded bit indentations, the strain applied to the polymer film during the reading/scanning operation, below T_g, must be minimized, and a higher shear modulus is desired. The higher modulus, assuming a constant adhesion force, will result in reduced friction forces, thus a reduced potential for wear.

The thermomechanical storage technique also requires specific attention to the local thermal transport properties of the polymer media and underlying substrate. Ideally, the heat transfer to the polymer should be limited only to the indentation site so adjacent data bits are not subject to thermal degradation, and the excess heat should be removed through the supporting substrate, a heat sink. This requires that the polymer medium has a very low thermal conductivity relative to the substrate. The heat transfer from the probe tip to the polymer is highly nonlinear, making it very difficult to reproducibly control tip penetration into the polymer, and hence, to maintain small uniform bit indentations. In order to overcome this difficulty, the depth of the tip penetration must be limited. The use of ultra-thin polymer films (<100nm) on a hard impenetrable substrate is a necessary and sufficient means to limit tip penetration. With this configuration, the hard substrate prevents the tip from penetrating farther than the film thickness.

Each indented bit generated with the TDS process represents a metastable state of the deformed volume, and will either initiate spontaneous dewetting (film instability) or strive for recovery of the initial unstressed state (bit instability). The delicate balance between these instability nodes constitutes one optimization scenario in the design of polymeric storage media. Furthermore, media (and data) wear must be minimized during scanning operations. In particular, topographical protrusions, in the form of piled-up *rims* around the indented bits, Fig. 4-20 (*Right*), are regions susceptible to wear. The presence of rims also adversely affects the writing density. Rims interact non-linearly with adjacent bits, lowering the signal-to-noise ratio of bit detection and requiring a relaxation of the indentation pitch (data density). From the perspectives of media wear and data density, a suitable polymer storage media exhibits a weak propensity for rim formation during indentation. Interfacially constrained systems like TDS, are impacted during indentation by material rheological gradients (i.e., $T_g(\delta)$ profile) in addition to mechanical constraints (illustrated in Fig. 4-21) from the underlying substrate. The combined influence of rigid dimensional constraints and material anisotropy during indentation has been addressed in our research with high-rate, SPM indentation studies typical of the TDS process.[29,31]

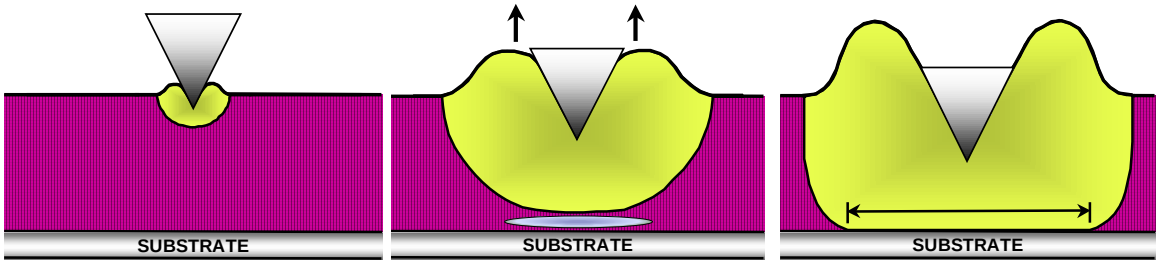

Fig. 4-21: Evolution of the plastic zone: (*Left*) Bulk behavior (self similarity), (*Middle*) Strain shielding (substrate effect, results in enhanced rim formation), (*Right*) confined plasticity (interfacial shear behavior).

A representative indentation is presented in Figure 4-22(Left) Our research showed that the rim height ζ is influenced by both process conditions (e.g. normal force, F_N) and the film thickness, and scales with the indentation depth h. Thus, substrate constraints are best assessed via the ratio of the rim height to the indent depth, ζ/h. In Figure 4-22(*Right*), the load normalized height to depth ratios, $\overline{\zeta / h}$, are reported for indentations in thin polystyrene films (M_w = *12k*). For film thicknesses, δ, exceeding ~100 nm, the $\overline{\zeta / h}$ ratio displays a constant value, which reflects the bulk material response. For film thicknesses below 100 nm, the rim height increases with decreasing film thickness. This behavior depends on the substrate material. The rim

enhancements were effectively masked by adding a compliant 230 nm thick crosslinked buffer film polystyrene-benzocyclobutane (PS-BCB) between the rigid substrate and the indented PS film. It is important to note that the indentation depth was less than 10 % of the film thickness, which excludes strain shielding effects as cause for the increase in rim heights below 100 nm thick films.

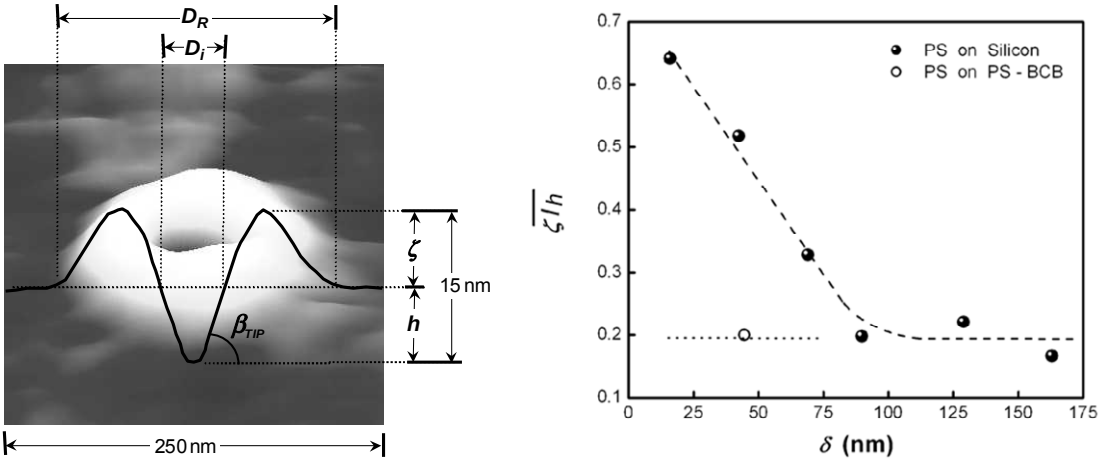

Fig. 4-22: (*Left*) AFM image of a residual indentation in polystyrene with rim height, ζ; indentation depth, h; rim diameter, D_R; and indentation diameter, D_i. (*Right*) Strain shielding at the substrate interface is evident in the load normalized ratio of rim height to indentation depth ($\overline{\zeta/h}$). For PS on a rigid silicon substrate, rim heights are enhanced for films thinner than 100 nm. A compliant PS-BCB buffer masks the substrate constraints.

A final analysis, in which we compared the effective modulus of indentation with the change in the glass transition, at last disclosed the underlying molecular origin for the enhancement of the rim.[31] Thereby, we compared the phenomenological *effective modulus* that the indenter experiences during an indentation with the local glass transition $T_g(\delta)$.The combined plot of the two quantities as function of the film thickness, Fig. 4-23, reveals the significant qualitative similarity between the modulus and T_g. Thus, viewing the glass transition as a molecular mobility barrier (c.f. sec. 2.1), the molecular mobility strongly affects the TDS process. As higher mobility (more precise a positive $d(T_g(\delta))/d\delta$ gradient) leads to smaller rim heights the critical thickness δ_{max} represents an important engineering parameter for TDS. First important steps have been explored by our group in collaboration with IBM on crosslinked material as discussed in subsection 2.2,

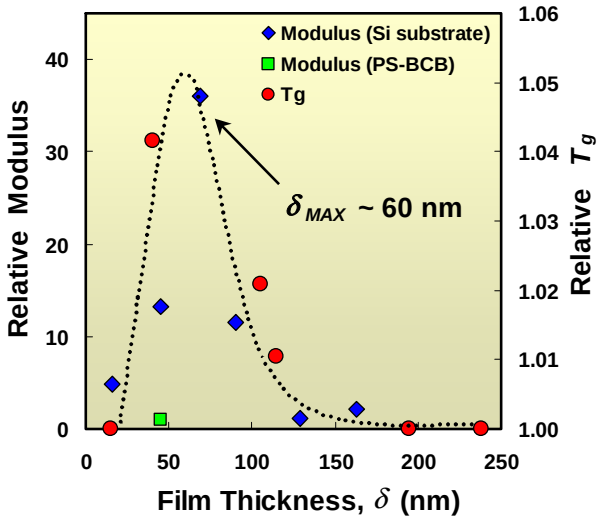

Fig. 4-23: Combination plot of the effective modules and the local glass transition. The qualitative correspondence is reflective of the impact of local mobility changes on the indentation mechanics.

With the TDS NEMS application we investigated an ultrahigh density recording scheme that is strongly affected by the underlying molecular mobility in the heterogeneous interfacial region of materials. In summary, our applied research towards devices in opto-electronics, membrane technology and NEMS illustrates the wide applicability of our research on intra/intermolecular and interfacial/dimensional constraints in materials.

6. References and Citations Therein

[1] D. B. Knorr, T. Gray, and R. M. Overney, *Cooperative and Submolecular Dissipation Mechanisms of Sliding Friction in Complex Organic Systems*, J. Chem. Phys. **129**, 074504 (2008).

[2] M. Y. He, A. S. Blum, G. Overney, and R. M. Overney, *Effect of interfacial liquid structuring on the coherence length in nanolubrication*, Physical Review Letters **88**, 154302 (2002).

[3] T. Gray, T. D. Kim, D. B. Knorr, J. D. Luo, A. K. Y. Jen, and R. M. Overney, *Mesoscale dynamics and cooperativity of networking dendronized nonlinear optical molecular glasses*, Nano Letters **8**, 754-9 (2008).

[4] D. B. Knorr, T. Gray, and R. M. Overney, *Intrinsic Friction Analysis - Novel Nanoscopic Access to Molecular Mobility in Constrained Organic Systems*, Ultramicroscopy **in press** (2008).

[5] R. M. Overney, E. Meyer, J. Frommer, D. Brodbeck, R. Luthi, L. Howald, H. J. Guntherodt, M. Fujihira, H. Takano, and Y. Gotoh, *Friction Measurements on Phase-Separated Thin-Films with a Modified Atomic Force Microscope*, Nature **359**, 133-5 (1992).

[6] T. Gray, R. M. Overney, M. Haller, J. Luo, and A. K. Y. Jen, *Low temperature relaxations and effects on poling efficiencies of dendronized nonlinear optical side-chain polymers*, Applied Physics Letters **86** (2005).

[7] S. Sills, R. M. Overney, W. Chau, V. Y. Lee, R. D. Miller, and J. Frommer, *Interfacial glass transition profiles in ultrathin, spin cast polymer films*, Journal of Chemical Physics **120**, 5334-8 (2004).

[8] S. Sills, T. Gray, and R. M. Overney, *Molecular dissipation phenomena of nanoscopic friction in the heterogeneous relaxation regime of a glass former*, Journal of Chemical Physics **123** (2005).

[9] R. Overney and E. Meyer, *Tribological Investigations Using Friction Force Microscopy*, Mat. Res. Soc. Bulletin **18**, 26-34 (1993).

[10] T. Gray, J. Killgore, J. D. Luo, A. K. Y. Jen, and R. M. Overney, *Molecular mobility and transitions in complex organic systems studied by shear force microscopy*, Nanotechnology **18** (2007).

[11] R.M. Overney and S. E. Sills, in *Interfacial Properties on the Submicron Scale*, edited by J. Frommer and R. M. Overney (Oxford Univ. Press, New York, 2001), p. 2-23.

[12] R. M. Overney, D. P. Leta, L. J. Fetters, Y. Liu, M. H. Rafailovich, and J. Sokolov, *Dewetting dynamics and nucleation of polymers observed by elastic and friction force microscopy*, Journal of Vacuum Science & Technology B **14**, 1276-9 (1996).

[13] R. M. Overney, G. Tindall, and J. Frommer, in *Handbook of Nanotechnology*, edited by B. Bhushan (1439-1453, Heidelberg, 2007).

[14] S. R. Ge, L. T. Guo, M. H. Rafailovich, J. Sokolov, R. M. Overney, C. Buenviaje, D. G. Peiffer, and S. A. Schwarz, *Wetting behavior of graft copolymer substrate with chemically identical homopolymer films*, Langmuir **17**, 1687-92 (2001).

[15] A. Karim, T. M. Slawecki, S. K. Kumar, J. F. Douglas, S. K. Satija, C. C. Han, T. P. Russell, Y. Liu, R. Overney, O. Sokolov, and M. H. Rafailovich, *Phase-separation-induced surface patterns in thin polymer blend films*, Macromolecules **31**, 857-62 (1998).

[16] C. Buenviaje, S. R. Ge, M. Rafailovich, J. Sokolov, J. M. Drake, and R. M. Overney, *Confined flow in polymer films at interfaces*, Langmuir **15**, 6446-50 (1999).

[17] R. M. Overney, C. Buenviaje, R. Luginbuhl, and F. Dinelli, *Glass and structural transitions measured at polymer surfaces on the nanoscale*, Journal of Thermal Analysis and Calorimetry **59**, 205-25 (2000).

[18] S. Ge, Y. Pu, W. Zhang, M. Rafailovich, J. Sokolov, C. Buenviaje, R. Buckmaster, and R. M. Overney, *Shear modulation force microscopy study of near surface glass transition temperatures*, Physical Review Letters **85**, 2340-3 (2000).

[19] E. Meyer, R. Overney, R. Luthi, D. Brodbeck, L. Howald, J. Frommer, H. J. Guntherodt, O. Wolter, M. Fujihira, H. Takano, and Y. Gotoh, *Friction Force Microscopy of Mixed Langmuir-Blodgett-Films*, Thin Solid Films **220**, 132-7 (1992).

[20] E. Meyer, R. Overney, D. Brodbeck, L. Howald, R. Luthi, J. Frommer, and H. J. Guntherodt, *Friction and Wear of Langmuir-Blodgett-Films Observed by Friction Force Microscopy*, Physical Review Letters **69**, 1777-80 (1992).

[21] L. Howald, R. Luthi, E. Meyer, G. Gerth, H. G. Haefke, R. Overney, and H. J. Guntherodt, *Friction Force Microscopy on Clean Surfaces of NaCL, NaF, and AgBr*, Journal of Vacuum Science & Technology B **12**, 2227-30 (1994).

[22] R. M. Overney, T. Bonner, E. Meyer, M. Reutschi, R. Luthi, L. Howald, J. Frommer, H. J. Guntherodt, M. Fujihara, and H. Takano, *Elasticity, Wear, and Friction Properties of Thin Organic Films Observed with Atomic-Force Microscopy*, Journal of Vacuum Science & Technology B **12**, 1973-6 (1994).

[23] R. M. Overney, H. Takano, M. Fujihira, W. Paulus, and H. Ringsdorf, *Anisotropy in Friction and Molecular Stick-Slip Motion*, Physical Review Letters **72**, 3546-9 (1994).
[24] R. M. Overney, H. Takano, and M. Fujihira, *Elastic Compliances Measured by Atomic-Force Microscopy*, Europhysics Letters **26**, 443-7 (1994).
[25] R. M. Overney, H. Takano, M. Fujihira, E. Meyer, and H. J. Guntherodt, *Wear, Friction and Sliding Speed Correlations on Langmuir-Blodgett-Films Observed by Atomic-Force Microscopy*, Thin Solid Films **240**, 105-9 (1994).
[26] F. Dinelli, C. Buenviaje, and R. M. Overney, *Glass transitions of thin polymeric films: Speed and load dependence in lateral force microscopy*, Journal of Chemical Physics **113**, 2043-8 (2000).
[27] C. Buenviaje, F. Dinelli, and R. M. Overney, *Investigations of heterogeneous ultrathin blends using lateral force microscopy*, Macromolecular Symposia **167**, 201-12 (2001).
[28] S. Sills and R. M. Overney, *Creeping friction dynamics and molecular dissipation mechanisms in glassy polymers*, Physical Review Letters **91**, 095501 (2003).
[29] S. Sills, H. Fong, C. Buenviaje, M. Sarikaya, and R. M. Overney, *Thermal transition measurements of polymer thin films by modulated nanoindentation*, Journal of Applied Physics **98** (2005).
[30] S. Sills, T. Gray, J. Frommer, and R. M. Overney, in *Applications of Scanned Probe Microscopy to Polymers*, 2005), Vol. 897, p. 98-111.
[31] S. Sills, R. M. Overney, B. Gotsmann, and J. Frommer, *Strain shielding and confined plasticity in thin polymer films: Impacts on thermomechanical data storage*, Tribology Letters **19**, 9-15 (2005).
[32] J. P. Killgore and R. M. Overney, *Interfacial mobility and bonding strength in nanocomposite thin film membranes*, Langmuir **24**, 3446-51 (2008).
[33] R. M. Overney, D. P. Leta, C. F. Pictroski, M. H. Rafailovich, Y. Liu, J. Quinn, J. Sokolov, A. Eisenberg, and G. Overney, *Compliance measurements of confined polystyrene solutions by atomic force microscopy*, Physical Review Letters **76**, 1272-5 (1996).
[34] M. Y. He, A. S. Blum, D. E. Aston, C. Buenviaje, R. M. Overney, and R. Luginbuhl, *Critical phenomena of water bridges in nanoasperity contacts*, Journal of Chemical Physics **114**, 1355-60 (2001).
[35] S. Sills, K. Vorvolakos, M.K. Chaudhury, and R. M. Overney, in *Friction and Wear on the Atomic Scale*, edited by E. Gnecco and E. Meyer (Springer Verlag, Heidelberg, 2007), p. 659-76.
[36] E. Meyer, L. Howald, R. M. Overney, H. Heinzelmann, J. Frommer, H. J. Guntherodt, T. Wagner, H. Schier, and S. Roth, *Molecular-Resolution Images of Langmuir-Blodgett-Films Using Atomic Force Microscopy*, Nature **349**, 398-400 (1991).
[37] R. Luthi, R. M. Overney, E. Meyer, L. Howald, D. Brodbeck, and H. J. Guntherodt, *Measurements on Langmuir-Blodgett-Films by Friction Force Microscopy*, Helvetica Physica Acta **65**, 866-7 (1992).
[38] F. Schabert, A. Hefti, K. Goldie, A. Stemmer, A. Engel, E. Meyer, R. Overney, and H. J. Guntherodt, *Ambient-Pressure Scanning Probe Microscopy of 2d Regular Protein Arrays*, Ultramicroscopy **42**, 1118-24 (1992).
[39] J. Frommer, R. Luthi, E. Meyer, D. Anselmetti, M. Dreier, R. Overney, H. J. Guntherodt, and M. Fujihira, *Adsorption at Domain Edges*, Nature **364**, 198- (1993).
[40] R. M. Overney, E. Meyer, J. Frommer, H. J. Guntherodt, M. Fujihira, H. Takano, and Y. Gotoh, *Force Microscopy Study of Friction and Elastic Compliance of Phase-Separated Organic Thin-Films*, Langmuir **10**, 1281-6 (1994).
[41] R. M. Overney, manuscript in preparation.
[42] T. Gray, C. Buenviaje, R. M. Overney, S. A. Jenekhe, L. X. Zheng, and A. K. Y. Jen, *Nanorheological approach for characterization of electroluminescent polymer thin films*, Applied Physics Letters **83**, 2563-5 (2003).
[43] T. D. Kim, J. W. Kang, J. D. Luo, S. H. Jang, J. W. Ka, N. Tucker, J. B. Benedict, L. R. Dalton, T. Gray, R. M. Overney, D. H. Park, W. N. Herman, and A. K. Y. Jen, *Ultralarge and thermally stable electro-optic activities from supramolecular self-assembled molecular glasses*, Journal of the American Chemical Society **129**, 488-9 (2007).
[44] J. H. Wei, M. Y. He, and R. M. Overney, *Direct measurement of nanofluxes and structural relaxations of perfluorinated ionomer membranes by scanning probe microscopy*, Journal of Membrane Science **279**, 608-14 (2006).
[45] J. P. Killgore, W. King, K. Kjoller, and R. M. Overney, *Heated-tip AFM: Applications in Nanocomposite Polymer Membranes and Energetic Materials*, Microscopy Today **15**, 20-5 (2007).